A report to the sponsors of the
Exploration Geophysics Laboratory

Processing Direct-S Data Produced by Vertical-Displacement Sources:

Data Polarity Concepts and Velocity Analysis Strategies

Bob Hardage

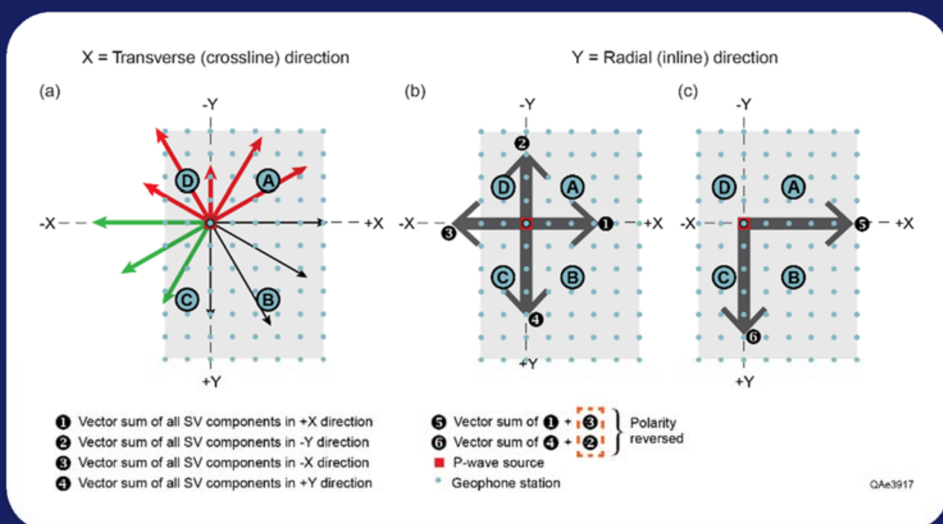

October 2015

EGL Exploration Geophysics Laboratory

Bureau of Economic Geology

QAe4126

Processing Direct-S Data Produced by Vertical-Displacement Sources: Data Polarity Concepts and Velocity Analysis Strategies

Bob A. Hardage
October 2015

Abstract

A vertical-displacement source is any seismic source that applies a vertical displacement to the earth to create wavefields for illuminating deep geology. Vertical-displacement sources include vertical vibrators, vertical impacts, and shot-hole explosives. Although these sources are considered to be conventional P-wave sources, they also generate robust direct-SV radiation.

This report describes principles that must be understood in order to process direct-S modes generated by these types of seismic sources. Direct-S waves are defined as S-waves produced directly at the point where the force vector generated by a seismic source interacts with the earth. These direct-S waves are fundamentally different from the popular P-SV (converted-S) modes produced by downgoing P waves at interfaces remote from a source station. Two types of direct-S imaging options are considered in this report. The first option is constructing S-S images from the direct-SV illumination produced by vertical-displacement sources. S-S data acquisition requires that 3C geophones be deployed because S-S reflections are recorded by horizontal geophones. The second option is SV-P (converted-P) imaging, which utilizes SV-to-P converted modes produced at remote interfaces by direct-SV modes generated by vertical-displacement sources. In contrast to S-S data, SV-P data are recorded by vertical geophones and involve a simpler, lower-cost, data-acquisition effort.

Adjusting S-wave data polarity and simplifying SV-P velocity analysis are the only topics considered in this data-processing report. Real-data examples are used to illustrate how the polarities of direct-SV modes produced by P-wave sources vary with azimuth. The method by which these azimuth-dependent direct-S polarities are adjusted to constant-polarity data during S-S data processing is then described. After this polarity adjustment, it is possible to make S-S images with vertical-displacement sources in the same way that S-S images are made with horizontal vibrators. It is emphasized several times that no data polarity adjustments are required to make SV-P images from P-source data recorded with vertical geophones.

P-P common-midpoint (CMP) constant-velocity panels are used to demonstrate a simple procedure that allows an approximate, first-order-accuracy SV-P velocity analysis to be done. Although constant-velocity stacks created by asymptotic-conversion-point (ACP) stacking are needed for SV-P velocity analysis, the procedure described in this report shows that valuable information about stacking velocities needed for SV-P imaging can be derived from P-P constant-velocity stacks of vertical-geophone data constructed with common-midpoint (CMP) binning procedures.

Introduction

Seismic data processing involves many issues such as static estimations, wavefield separation, velocity analysis, suppression of multiples, noise attenuation, migration, and other procedures. These data-processing issues expand in number and tend to be more complicated when processing seismic land data rather than marine data. The necessity to calculate source and receiver static corrections is one example of the increased challenges of processing land-based seismic data compared to processing marine data acquired with towed cables.

All of the issues that have to be overcome when processing land-based seismic data become greater challenges when land data involve S-wave data. For example, determining proper S-wave static corrections across some earth surfaces can be a greater challenge than estimating P-wave statics. S-wave static estimation is only one of several data-processing issues that will not be discussed in this report. These topics will be considered in subsequent reports to EGL sponsors.

Only two data-processing topics are considered in the following report sections: (1) azimuth-dependent polarities of direct-SV modes produced by P-wave sources and the procedures that must be taken to remedy the effects of these data polarities if S-S images are to be made, and (2) SV-P velocity analyses that need to be done to create optimal-quality converted-P images. Proper data polarities and accurate stacking velocities are essential when creating images with direct-SV modes produced by vertical-displacement sources. These two procedures (polarity adjustments and velocity analyses) are thus data-processing steps where mistakes must be avoided when processing direct-S modes produced by P-wave sources.

Direct-S Radiation Patterns

Direct-S waves are defined as S-waves produced directly at the coordinates where the displacement vector generated by a seismic source interacts with the earth. Direct-S modes are created when the direction of source displacement is horizontal, vertical, or slanted. Although the standard source used to generate direct-S waves is a horizontal vibrator (a horizontal-displacement source), the focus of this report is on direct-SV modes produced by vertical-displacement sources (vertical vibrator, vertical impact, shot-hole explosive). Field tests done at EGL show that vertical-displacement sources generate robust direct-S waves; however, these direct-S modes have a polarity behavior that differs from the polarities of direct-S modes produced by horizontal-displacement sources. The quality of S-S images made with direct-S modes produced by vertical-displacement sources depends on whether the polarities of direct-S data are properly managed.

The theoretical shapes of direct-P and direct-SV modes produced by a vertical-displacement source are illustrated in Figure 1. Mathematical calculations performed by Miller and Pursey (1954), White (1983), and others show radiation patterns similar to the results displayed in Figure 1. Similar examples of calculated P and S radiation patterns have been provided to EGL sponsors via internal EGL sponsor reports (Hardage and Wagner, 2014a, 2014b). In Figure 1, radiation patterns are shown for a soft earth (Figure 1a where Poisson's ratio is 0.44 [$V_P/V_S = 3$]) and for a relatively hard earth (Figure 1b where Poisson's ratio is 0.33 [$V_P/V_S = 2$]). For a homogeneous earth, the relationship between the V_P/V_S velocity ratio and Poisson's ratio (σ) within the propagation medium is given by Equation 1:

(1) $\sigma = [(V_P/V_S)^2 - 2] / [(2(V_P/V_S)^2 - 2]$.

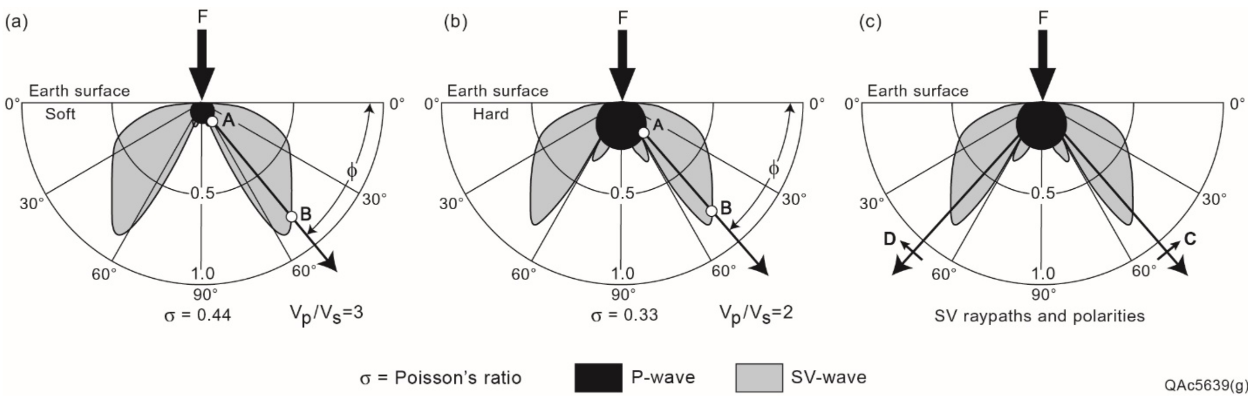

Figure 1. P and S radiation model for a vertical-displacement source. **F** is the force vector that creates the vertical displacement. (a) P and SV radiation for a relatively soft earth [$V_P/V_S = 3$]. (b) P and S radiation for a rather hard earth [$V_P/V_S = 2$]. The amplitude of P radiation at takeoff angle **Φ** is **A**, and the amplitude of SV radiation is **B**. (c) SV raypaths and SV displacement vectors for SV modes propagating in opposite-azimuth directions. SV polarity **C** is opposite to SV polarity **D** because the horizontal components of SV displacements associated with raypaths **C** and **D** point in opposing directions.

Important principles are shown by this radiation model. The first principle is that the amount of SV energy produced by a vertical-displacement source is larger than the amount of P energy produced by the source. This fact is demonstrated in Figures 1a and 1b where **A** is the amplitude of P-wave radiation propagating at takeoff angle **Φ**, and **B** is the amplitude of SV radiation traveling in the same takeoff-angle direction. The second principle is that the amplitude **B/A** increases as Poisson's ratio of the earth increases (i.e. as the V_P/V_S velocity ratio increases in the earth layer where a vertical-displacement source vector is applied). This S-wave illumination behavior indicates that a soft, unconsolidated surface can be beneficial for generating (and recording) robust direct-S modes.

The wave-mode radiation physics illustrated in Figure 1, which is correct only for a homogeneous earth, is reasonably representative of what EGL finds when direct-P and direct-S radiations are measured in real-earth conditions. The principal distinctions between the mathematically simulated radiation patterns in Figure 1 and what EGL observes in real-data radiation patterns are:

- There is indeed a reduction in direct-S amplitudes when takeoff angles are close to vertical, but the dramatic reduction in vertically traveling direct-S radiation shown in Figure 1 is usually not observed. Even though direct-S amplitudes that propagate at takeoff angles close to vertical are less than the direct-S amplitudes that propagate at takeoff angles of 30 to 60 degrees, we often observe that SV modes propagating in near-vertical directions have approximately the same magnitudes as their companion direct-P amplitudes that propagate in the same near-vertical takeoff angle directions.

- The **B/A** ratio of direct-P and direct-S amplitudes observed in real data has, to date, always been a magnitude that is greater than 1.0, as implied by Figure 1, but the ratio varies as a function of azimuth. This azimuth-dependent variation in direct-P and direct-S amplitudes is tentatively assumed to be caused by azimuth-dependent changes in stiffness coefficients local to source stations.

Topic 1: Polarity of Direct-SV Modes Produced by P-Wave Sources

SV raypaths and SV displacement vectors are added to the SV radiation patterns in Figure 1c to illustrate the first principle of direct-SV wave physics that will be discussed in this report. This first concept is that direct-SV modes that propagate away from a vertical-displacement source station in opposite-azimuth directions have opposite polarities if the data are recorded by similarity oriented horizontal geophones. The term “opposite-azimuth directions” means directions that have azimuths that differ by 180 degrees. This principle that opposite-polarity data are recorded by horizontal geophones occurs because the horizontal component of opposite-azimuth SV displacement vectors **C** and **D** point in opposite directions in Figure 1c.

These opposing orientations of the horizontal components of displacements **C** and **D** mean the polarity of reflected SV data recorded by horizontal geophones positioned left of vertical displacement **F** (negative-offset stations) is opposite to the polarity of reflected SV data recorded by horizontal geophones to the right of **F** (positive-offset stations). In contrast to the opposite-polarity behavior of positive-offset and negative-offset data acquired by horizontal geophones, SV-P modes recorded by vertical geophones at positive-offset and negative-offset stations have identical polarities. This principle is illustrated by the fact that the vertical components of displacement vectors **C** and **D** in Figure 1c both point upward.

S-S Imaging with P-Wave Sources

S-S Data Polarity

The distinction between opposite-azimuth polarity behavior of S-S data generated with vertical-displacement and horizontal-displacement sources will first be illustrated with synthetic model data and then will be verified by examining real-data examples. The modeling examples used here have been discussed in previous reports sent to EGL sponsors (Hardage and Wagner, 2014a, 2014b). These numerical calculations are presented again in this report as Figures 2 and 3 to illustrate how the polarities of direct-S reflections recorded at positive-offset and negative-offset receiver stations are determined by whether the receivers are oriented parallel to, or orthogonal to, the direction of the source displacement.

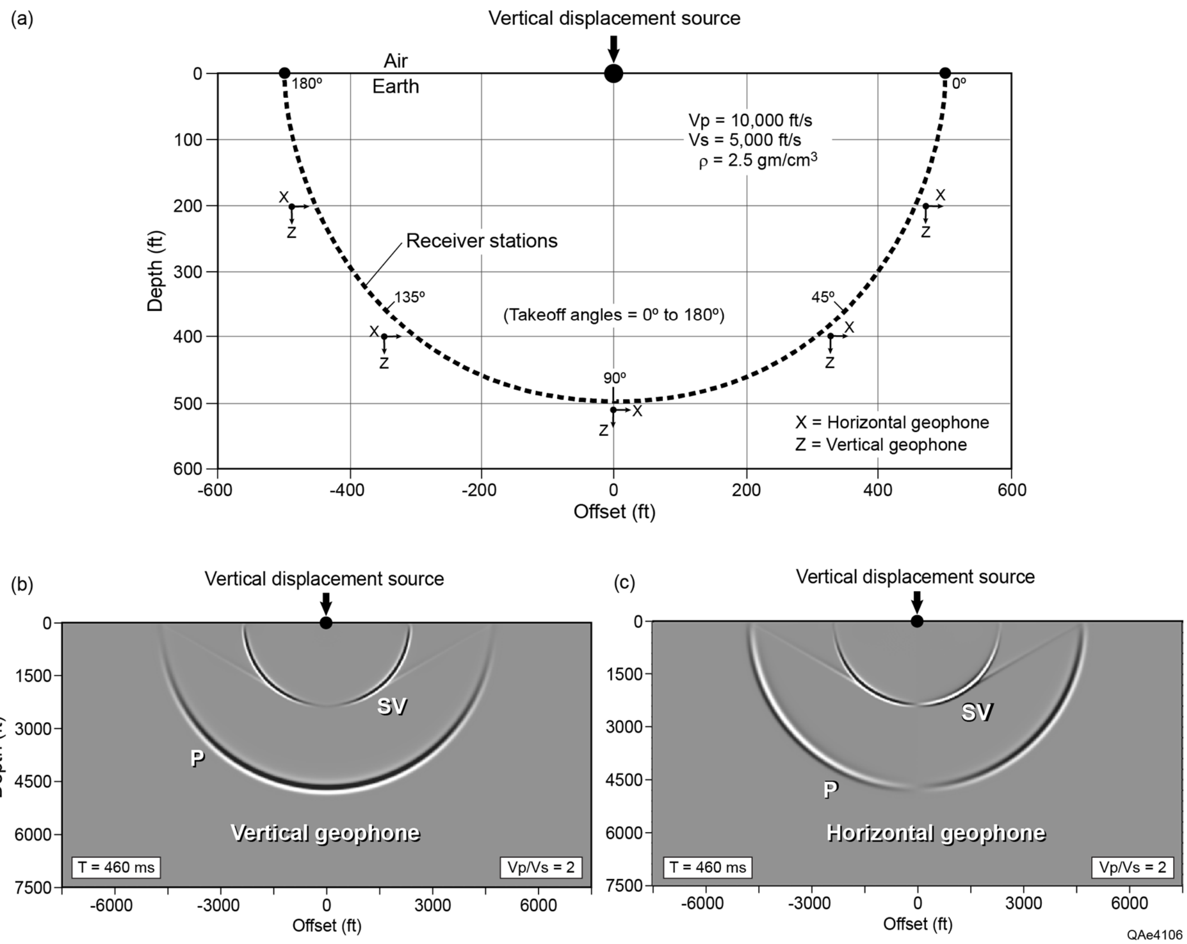

Figure 2. (a) Earth model used to calculate the polarities of direct-P and direct-S illuminating wavefields created by a vertical-displacement source. Vertical and horizontal geophones are moved outward from a surface-based source station on an expanding, constant-radius surface centered on that source station. Geophone stations forming a 500-ft semicircle are shown as an illustration. (b) P and SV propagating wavefronts recorded by vertical geophones when the receiver are 4600 ft from the source station. The polarities of P and SV wavefronts observed at positive-offset receiver stations have the same polarities as the wavefronts observed at negative-offset receiver stations. (c) P and SV propagating wavefronts recorded by radial-horizontal geophones when the receivers are 4600 ft from the source station The polarities of P and SV wavefronts observed at positive-offset receiver stations have opposite polarities to the wavefronts observed at negative-offset receiver stations. Taken from Hardage and Wagner (2014b).

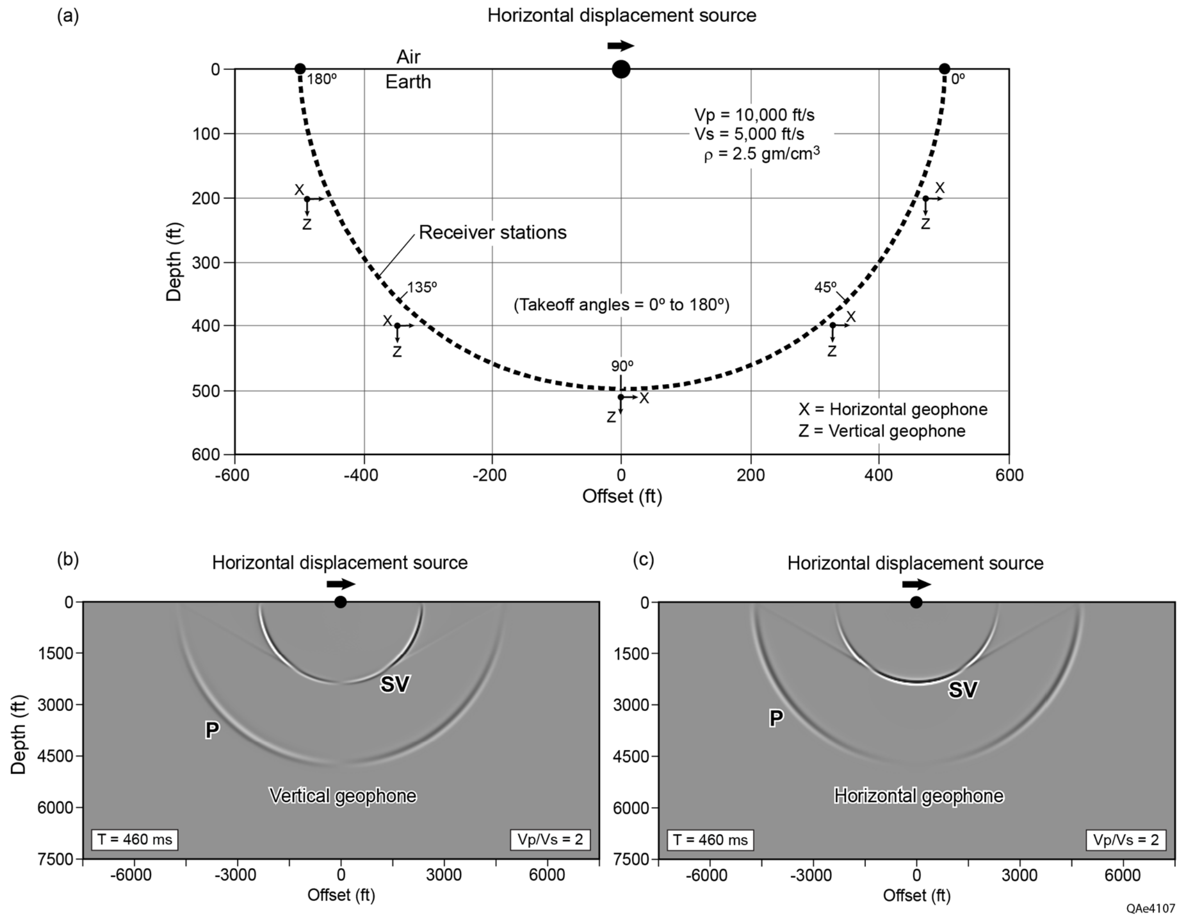

Figure 3. (a) Earth model used to calculate the polarities of direct-P and direct-S illuminating wavefields created by a horizontal-displacement source. Vertical and horizontal geophones are moved outward from a surface-based source station on an expanding, constant-radius surface centered on that source station. Geophone stations forming a 500-ft semicircle are shown for illustration. (b) P and SV propagating wavefronts recorded by vertical geophones when the receivers are 4600 ft from the source station. The polarities of P and SV wavefronts observed at positive-offset receiver stations have opposite polarities to the wavefronts observed at negative-offset receiver stations. (c) P and SV propagating wavefronts recorded by radial-horizontal geophones when the receivers are 4600 ft from the source station. The polarities of P and SV wavefronts observed at positive-offset receiver stations have the same polarities as the wavefronts observed at negative-offset receiver stations. Taken from Hardage and Wagner (2014b).

The earth model used in this analysis is illustrated in Figure 2a. Receivers are positioned on a buried, semi-circular surface centered on a surface-positioned source station. This semi-circular receiver surface expands as wavefronts propagate. Each receiver station is occupied by a vertical geophone and a radial-horizontal geophone. These receiver stations are positioned at takeoff angle increments of 1 degree that span the full takeoff-angle range of 0 to 180 degrees around the source station. This geophone spacing allows propagating wavefronts to be properly sampled in X-Y image space. Vertical geophones and horizontal geophones are oriented in the same directions at all receiver stations as shown by the few geophone diagrams distributed around the receiver surface. The propagation medium has a constant V_P velocity (10,000 ft/s) and a constant V_S velocity (5,000 ft/s) throughout its full extent.

The polarities of direct-P and direct-SV illuminating wavefronts recorded by the vertical geophones when the source-to-receiver distance is 4600 ft are shown in Figure 2b, and the polarities of direct-P and direct-SV wavefronts recorded by the radial-horizontal geophones are displayed as Figure 2c. Principles established by these wavefront calculations are:

1. If receivers are oriented in the same direction as the source displacement vector, the polarities of direct-P and direct-SV illuminating wavefronts at positive-offset receiver stations are the same as their polarities at negative-offset receiver stations. See Figure 2b that shows direct-P and direct-SV polarity behavior for vertical geophones and a vertical-displacement source vector.

2. If receivers are oriented orthogonal to the direction of the source displacement vector, the polarities of direct-P and direct-SV illuminating wavefronts at positive-offset receiver stations are opposite to their polarities at negative-offset receiver stations. See Figure 2c that shows direct-P and direct-SV polarity behavior for radial-horizontal geophones and a vertical source-displacement vector.

The diagram in Figure 3a shows the same earth model as Figure 2a. The only change is that the source station is now occupied by a horizontal-displacement source. The polarities of direct-P and direct-SV illuminating wavefields recorded by the vertical geophones after a travel distance of 4600 ft are shown in Figure 3b, and the polarities of direct-P and direct-SV reflections recorded by the radial-horizontal geophones are displayed as Figure 3c. The same principles stated above are re-established by these wavefront calculations:

3. If receivers are oriented orthogonal to the direction of the source displacement vector, the polarities of direct-P and direct-SV illuminating wavefronts at positive-offset receiver stations are opposite to their polarities at negative-offset receiver stations. See Figure 3b that shows polarity behavior for vertical geophones and a radial-horizontal source-displacement vector.

4. If receivers are oriented in the same direction as the source displacement vector, the polarities of direct-P and direct-SV illuminating wavefields at positive-offset receiver stations are the same as their polarities at negative-offset receiver stations. See Figure 3c that shows direct-P and direct-SV polarity behavior for radial-horizontal geophones and a radial-horizontal source displacement vector.

S-S Imaging

Real Data Examples of S-S Mode Polarities

Real data examples of direct-SV modes produced by vertical-displacement sources are presented in this section to verify the direct-SV reflection-polarity principles predicted by numerical modeling in Figure 2. These real-data examples involve vertical seismic profile (VSP) data, near-surface reflection profiles, and deep-geology reflection profiles.

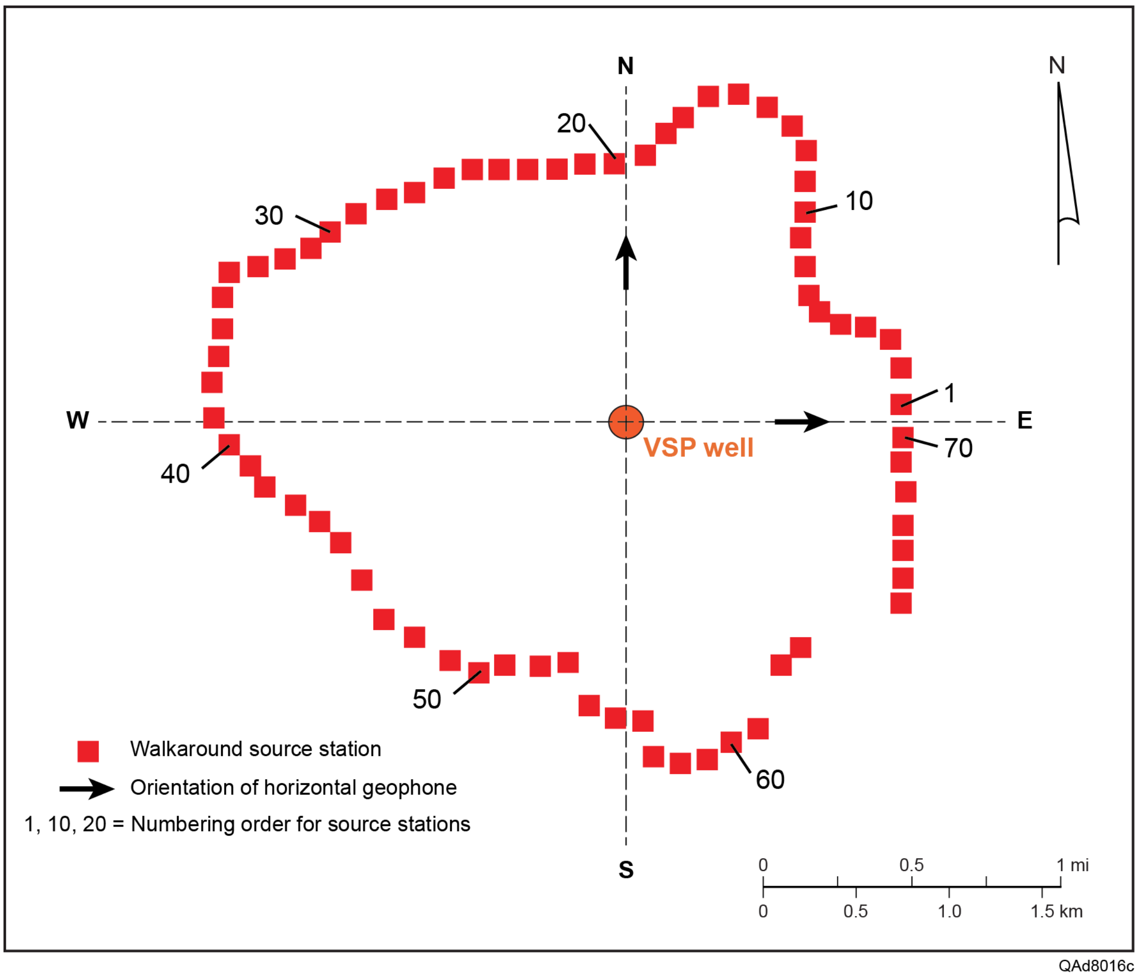

Figure 4. VSP source-receiver geometry used to verify direct-SV data polarity produced by a vertical-displacement source (a vertical vibrator in this case).

VSP Example

Vertical seismic profile (VSP) data offer a rigorous way to confirm azimuth-dependent polarity of direct-SV modes produced by vertical-displacement sources. The VSP data-acquisition program that created the data used in this discussion is illustrated in Figure 4. A 16-level array of 3C geophones was locked in place across a depth interval of 5820 to 6570 ft

(1774 to 2003 m) in the labeled well to record illuminating wavefields propagating away from a vertical vibrator successively positioned at each of the walk-around source stations. The receivers were not unlocked or moved during the data recording. Unfortunately a horizontal vibrator was not deployed for this VSP effort, which would have created an even more valuable set of source-test data.

Direct wavefields produced at two sets of opposite-azimuth source stations will be used to illustrate the opposite-azimuth data polarity of direct-P and direct-SV modes produced by a vertical vibrator. First, VSP geophones were rotated in the horizontal plane so that the H1 horizontal geophone at all 16 downhole receiver stations was oriented east (Figure 4). No receiver rotation was done in the vertical plane as is usually done when using VSP data for imaging purposes. The objective of this simpler horizontal-plane-only VSP receiver rotation was to create a vertical array of 3C geophones that replicated the orientations of 3C surface-deployed geophones; i.e., at each receiver station, one geophone was always vertical, one geophone was always in the same radial-horizontal orientation, and one geophone was always in the same transverse-horizontal orientation. The orientations of these geophones were not adjusted as sources were positioned in opposite-azimuth east and west directions from the VSP well.

Data recorded when a vertical vibrator was first positioned east of the VSP well and then moved to a station west of the well are shown in Figures 5a and 5b. The radial-horizontal geophones were oriented east as illuminating wavefields were generated at these two opposite-azimuth source stations. The direct-mode data recorded when the receiver was in a negative-offset direction from the east source station is displayed as Figure 5a, and the data recorded when the receiver was at a positive-offset coordinate relative to the west source station is shown in Figure 5b. The radial-horizontal geophone was then oriented north. Data acquired with this north-oriented horizontal geophone when the vertical-vibrator source station was north of the VSP well are shown in Figure 5c. The data created when the vertical vibrator was moved to a station south of this north-pointing horizontal geophone are shown as Figure 5d. In both of these VSP tests, the direct-SV first arrival has opposite polarity when vertical-vibrator data originate at opposite-azimuth source stations from a fixed receiver station.

Positive-offset and negative-offset direct-P data also have opposite polarity in this test (Figure 5) because the data are recorded by radial-horizontal geophones, not by vertical geophones. The data polarity behavior observed in this field test confirms the modeling result in Figure 2c that data polarity of positive-offset data (east or north source stations) is opposite to data polarity of negative-offset data (west or south source stations) if the orientations of source displacement and receiver axis are orthogonal (vertical source displacement and horizontal receiver in this case). This principle for orthogonal source and receiver axes applies to both direct-P and direct-SV wave modes. More important for purposes of S-S imaging with P-wave sources, the data in Figure 5 confirm that positive-offset and negative-offset direct-SV data produced by a vertical-displacement source have opposite polarity.

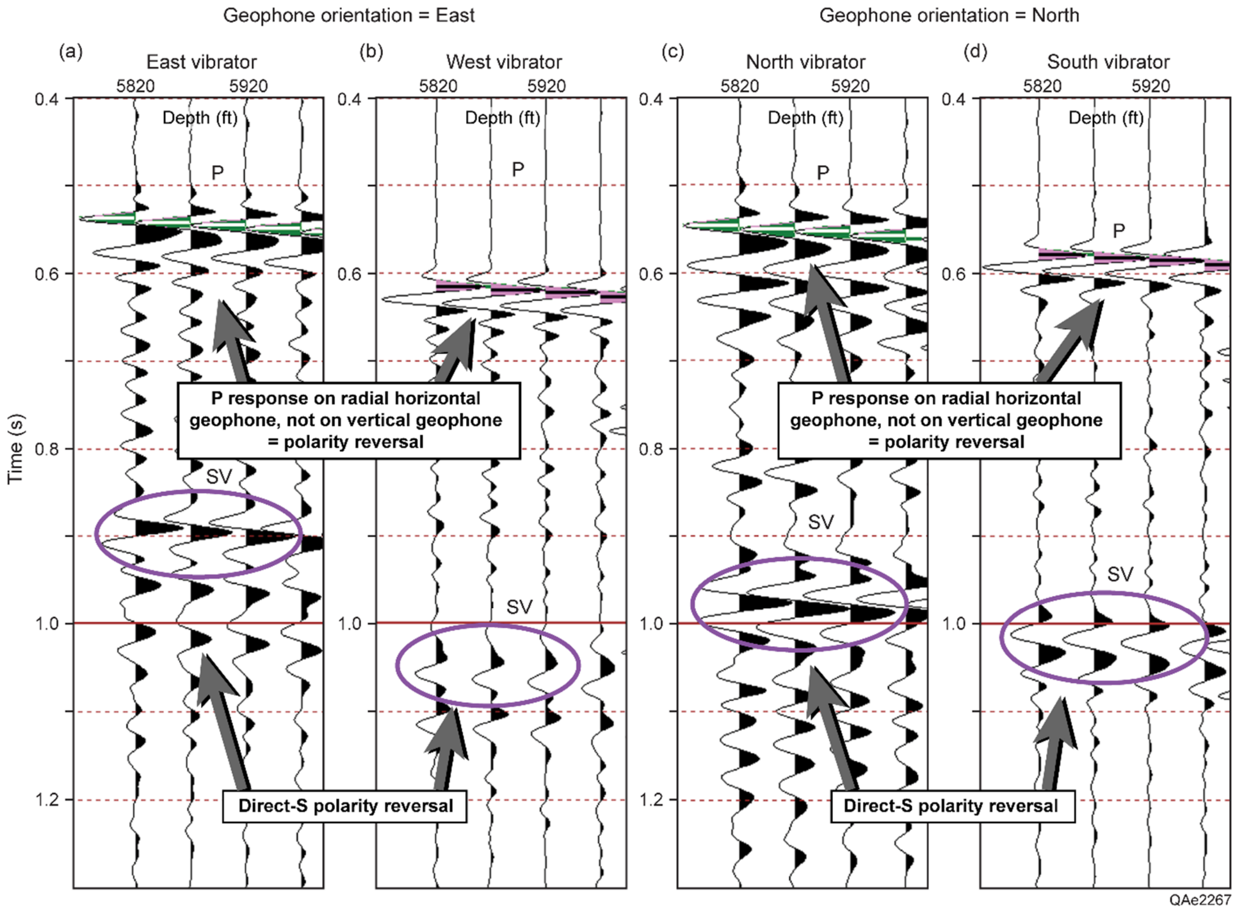

Figure 5. VSP test of direct-mode data polarity produced by a vertical-displacement source. (a) Response of radial-horizontal geophones oriented east and a vertical vibrator stationed east of the VSP well. (b) Response of the same radial-horizontal geophones with their east orientation but a vertical vibrator stationed west of the VSP well. (c) Response of radial-horizontal geophones oriented north and a vertical vibrator stationed north of the VSP well. (d) Response of the same radial-horizontal geophones in their north orientation but a vertical vibrator stationed south of the VSP well.

Near-Surface Example

Guy (2004) published a near-surface seismic study in which he presented examples of common-shot gathers generated by a vertical vibrator and a horizontal vibrator. Some of his test data are exhibited in Figure 6. These data were recorded as a 2D profile of source and receiver stations. Both horizontal and vertical vibrators were deployed at the source stations, and data were recorded with 3C geophones. Data generated by a radial-horizontal vibrator and a vertical vibrator and recorded by radial-horizontal geophones are shown as Figures 6a and 6b, respectively. Data generated by a transverse-horizontal vibrator and a vertical vibrator and recorded by transverse-horizontal geophones are then shown as Figures 6c and 6d.

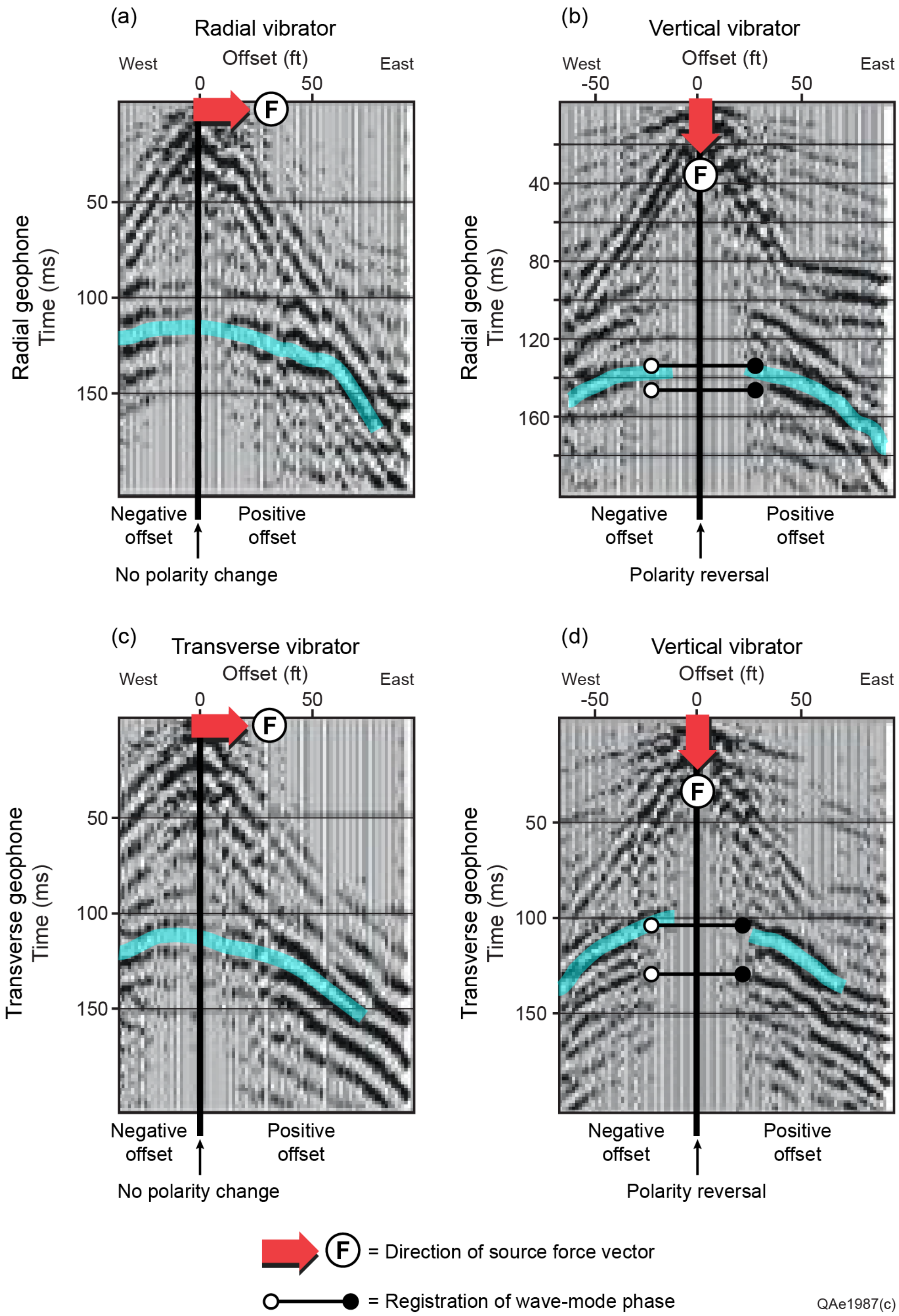

Figure 6. Near-surface shot gathers illustrating polarity differences between direct-S modes generated by horizontal-displacement sources and vertical-displacement sources. The bold red arrow **F** on each panel indicates the direction in which the source displaces the earth. Data examples involve: (a) a radial-horizontal vibrator and radial-horizontal geophones, (b) vertical vibrator and radial-horizontal geophones, (c) transverse-horizontal vibrator and transverse-horizontal geophones, and (d) vertical vibrator and transverse-horizontal geophones. Taken from Guy, 2004.

The term “radial” in these data displays means the horizontal geophone (or the displacement of the horizontal vibrator) was oriented in the vertical plane that follows the surface track of the 2D profile. The term “transverse” means the horizontal geophone (or the displacement of the horizontal vibrator) was oriented perpendicular to this same vertical plane.

In each shot-gather data panel, positive-offset direct-S data produced by the vertical vibrator are opposite-azimuth data relative to negative-offset data. Selected direct-S reflections are shaded blue to aid visual comparisons of the polarity behavior of direct-S modes produced by horizontal-displacement and vertical-displacement vibrators in these opposite-azimuth data traces. Weak S-S reflections produced by the horizontal vibrator can be seen spanning near-offset distances of -15 ft to +15 ft (-4.6 m to +4.6 m) in Figures 6a and 6c, and the amplitudes of these reflections increase with increasing offset. These examples confirm that direct-S reflections generated by a horizontal-displacement source have identical polarities in opposite-azimuth directions if the reflections are recorded by horizontal-axis sensors.

Note that the radiation strength of the direct-S reflections from the horizontal vibrator weakens at short-offset receiver stations because of the trace scaling that is used for the wiggle-trace displays (Figures 6a and 6c). S-S reflections produced by the vertical vibrator are even weaker across this same short-offset range because of the data scaling used for display purposes (Figures 6b and 6d). In EGL’s experience, weaker-amplitude S reflections are commonly seen near vertical takeoff angles from a vertical vibrator source station, compared to reflection amplitudes at non-vertical takeoff angles, because of the SV radiation geometry exhibited in Figure 1. However in most real-data examples, EGL observes that although SV illuminating amplitudes are weaker at near-vertical takeoff angles from vertical-displacement source stations, those SV amplitudes are still approximately the same magnitude as direct-P amplitudes propagating in the same takeoff angle direction.

Horizontal red lines are drawn on Figures 6b and 6d to show how reflection phase at a selected positive-offset distance compares with the reflection phase at the same offset distance in the negative-offset direction. This method of interpreting reflection polarity demonstrates that S-S reflections generated by a vertical vibrator have opposite polarities in opposite-azimuth directions. This real-data behavior is identical to the principle demonstrated in the numerical calculation summarized in Figure 2c – *if the source displacement and the sensor axis are orthogonal (as in Figures 6b and 6d) then S-S reflections have opposite polarities in negative-offset and positive-offset directions.*

These near-surface data examples are particularly important because they illustrate the extremely shallow depth below a vertical-vibrator station where fully developed direct-S modes can be observed. Perhaps the strongest evidence that S-S reflections in the vertical-vibrator data (Figures 6b and 6d) are produced by an S mode generated directly at the vertical-vibrator source station, not by P-to-SV conversion at an interface near the source station as some claim, is the observation that the reflections have the same arrival times as the S-S reflections seen in the horizontal-vibrator data (Figures 6a and 6c). If these two sets of S-S reflections appear at the same arrival times, then the illuminating S wavefields produced by a vertical vibrator have to be created at the same depth coordinate as the illuminating S wavefields produced by a horizontal vibrator.

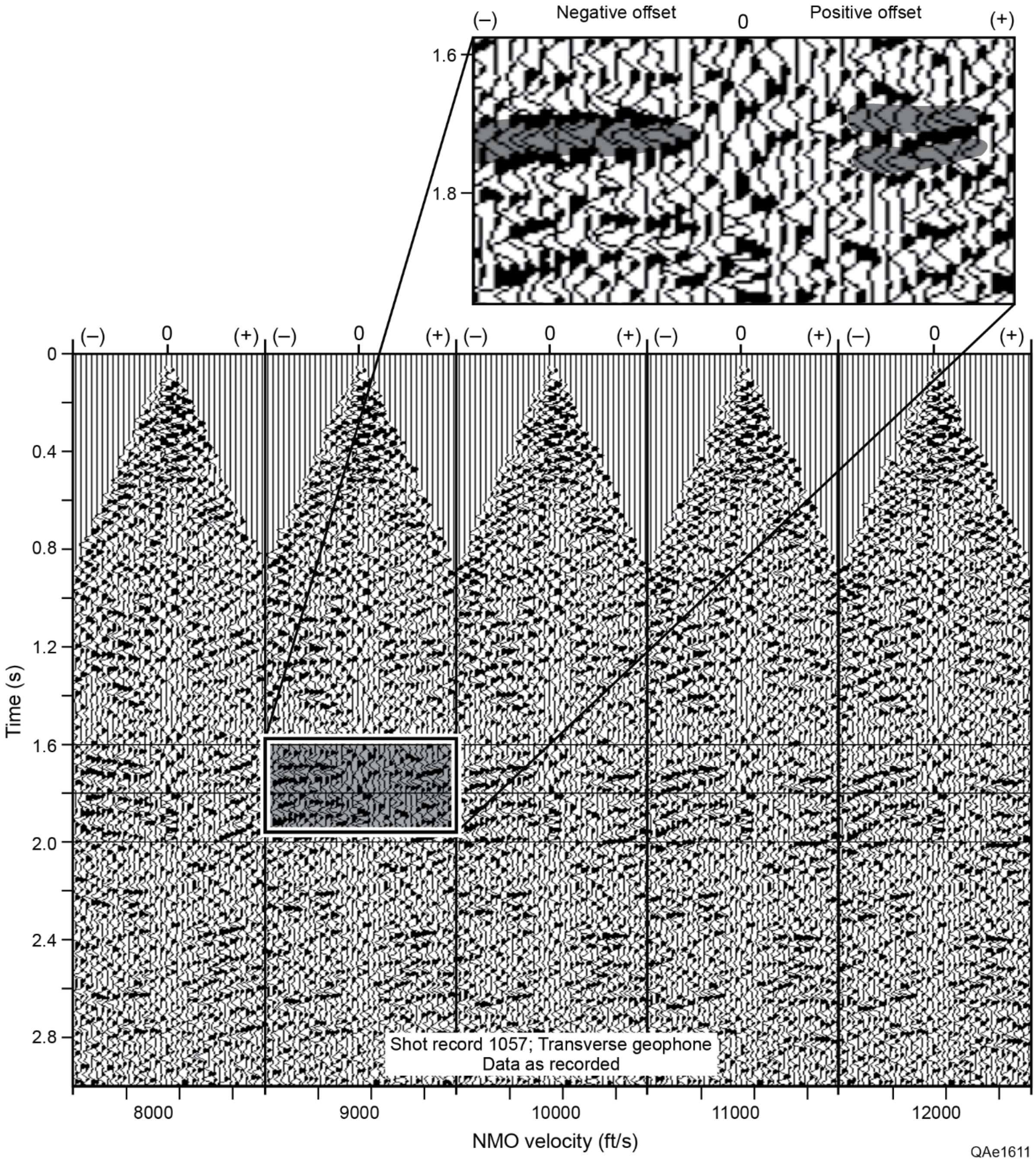

Figure 7. Constant-velocity CMP stacks of data generated by shot-hole explosives and recorded by surface-based transverse-horizontal geophones. The trace gathers used in this velocity analysis were created from transverse-horizontal geophone data in their raw, "as recorded" state and show the opposite-polarity behavior of opposite-azimuth data generated by a vertical-displacement source (zoom window).

Example Using Surface-Based Seismic Data

Shot-hole explosives are also a type of vertical-displacement (P-wave) source. The example of explosive-source data exhibited in Figure 7 illustrates the polarity behavior of opposite-azimuth, vertical-displacement source data acquired with surface-based receivers. In this case, the surface receivers were transverse-horizontal geophones, meaning the horizontal geophones were oriented perpendicular to the plane of the data display. Each data panel shows the effect of applying a constant-velocity normal moveout (NMO) correction to common-source trace gathers. The velocity used in each NMO correction of the reflection events is labeled below each panel. The robust S-S reflection at approximately 1.7 sec allows the effect of each NMO correction to be evaluated. Examination of the data shows an NMO velocity of approximately 9000 ft/s (2743 m/s) is appropriate for stacking reflection events near an image time of 1.7 sec (zoom window display).

The source position (zero-offset distance) is indicated by the number zero at the top of each panel; the positive-offset direction is indicated with a plus sign; and the negative-offset is labeled with a negative sign. The highlighted reflection event in the zoom window (Figure 7) shows that positive-offset data and negative-offset data have opposite polarities. Thus stacking S-S reflections produced by a vertical-displacement source will be a destructive process, not a constructive process, unless the polarity of negative-offset data is reversed to agree with the polarity of positive-offset data. This principle is again illustrated in Figure 8 where positive-offset and negative-offset data are stacked without reversing the polarity of the negative-offset data (Figure 8a) and then stacked after the polarity of negative-offset data is reversed (Figure 8b). The improvement in reflection signal quality in Figure 8b is obvious.

The fact that the data in Figure 8a show evidence of S-S reflections may mislead some data processors. A data processor may assume no data polarity issues exist if reflections appear in constant-velocity stacks without doing any adjustments to data polarity. However, the difficulty of estimating S-wave statics will increase, and only sub-standard S-S images can be created if data-polarity is not properly adjusted. Even if a S-S image is produced without reversing the polarity of negative-offset data, the image will be inferior to the image that will result when negative-offset S-S polarity is adjusted to agree with positive-offset S-S polarity. Note in particular that a data processor may not select a proper stacking velocity (based on optimal reflection flatness) when data polarities are not properly adjusted (Figure 8a) but can do so when it is recognized that opposite-offset data have opposite polarities (Figure 8b).

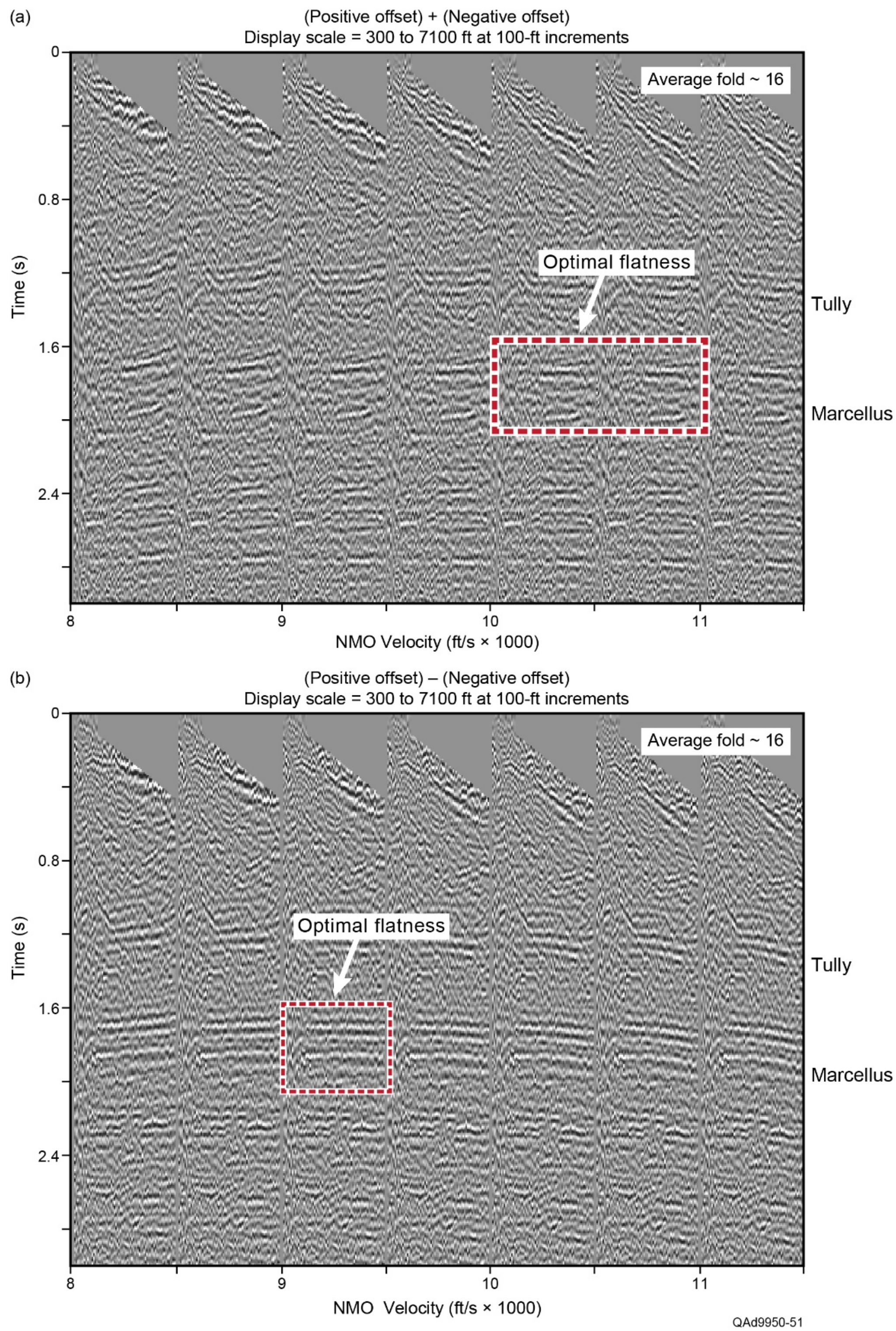

Figure 8. Constant-velocity panels of stacked data generated by shot-hole explosives and recorded by transverse-horizontal geophones. (a) Data stacked without altering the polarity of opposite-azimuth data. A deceptive outcome in this example is that several reflections can be seen. The evidence of these reflections may cause data processors to assume data polarity is correct. (b) Data stacked after reversing the polarity of negative-offset data. Reflections now have increased signal quality and improved continuity. Also note how the choice of optimal stacking velocity (dashed boxes) reduces to slower velocities when direct-SV data polarity is properly handled.

<u>Direct-SV Polarity Corrections Required for Surface-Recorded P-Source Data</u>

The data examples presented in Figures 7 and 8 confirm that direct-SV data generated by a vertical-displacement source (vertical vibrator, vertical impact, shot-hole explosive) and recorded by horizontal geophones have opposite polarity in opposite-azimuth directions away from a source station. This polarity behavior differs from that which would result if two orthogonal horizontal-displacement sources (e.g. two orthogonal horizontal vibrators) are deployed at source stations. Two orthogonal horizontal vibrators would create direct-S modes that have the same polarity in opposite-azimuth directions away from a source station. This fundamental principle is illustrated in Figure 3c.

It is essential that at every source station in a 3D survey that the polarity of direct-SV modes created by a vertical-displacement source be converted to the same data-polarity behavior as that which would be produced by two orthogonal horizontal-displacement sources at the same source stations. This data polarity adjustment must be done at an early point in a data-processing flow before attempts are made to determine S-S static corrections or to estimate S-S stacking velocities. The diagram in Figure 9 illustrates how this polarity correction, when applied to 3D data, results in constant-polarity S-S data equivalent to the S-S data polarity created by the standard approach of deploying two orthogonal horizontal vibrators to perform S-S imaging.

The diagram in Figure 9a is a map view of the polarity behavior of direct-SV modes propagating away from a P-source station. Each arrow pointing away from the source station indicates the polarity orientation of the direct-SV mode that propagates in that azimuth direction, and the length of each arrow indicates the amplitude strength of the direct-SV displacement in that same propagation direction. This azimuth-dependent polarity and radiation strength represent direct-SV waves propagating in a layered medium in which there are azimuthal variations in stiffness coefficients. The data space around each source station will be defined in terms of inline (**Y**) and crossline (**X**) coordinates for the total 3D survey. The orientation of the inline coordinate axis is commonly defined as the direction in which receiver lines are deployed, but this definition can be adjusted by data processers if they wish to do so.

The seismic image space around each source station is divided into negative-offset (**-X**) and positive-offset (**+X**) crossline data space and negative-offset (**-Y**) and positive-offset (**+Y**) inline data space. For convenience, the data space around each source station will also be divided into quadrants **A, B, C,** and **D** as shown in Figure 9. The sequence order in which SV data polarity is adjusted in these quadrants is arbitrary. For this discussion, SV data polarity in source-space **(+X,+Y)**, which is data space quadrant **B** in Figure 9, will be selected as the data polarity desired for all illuminating direct-SV wavefields that radiate away from all source stations that are deployed across this 3D data-acquisition space.

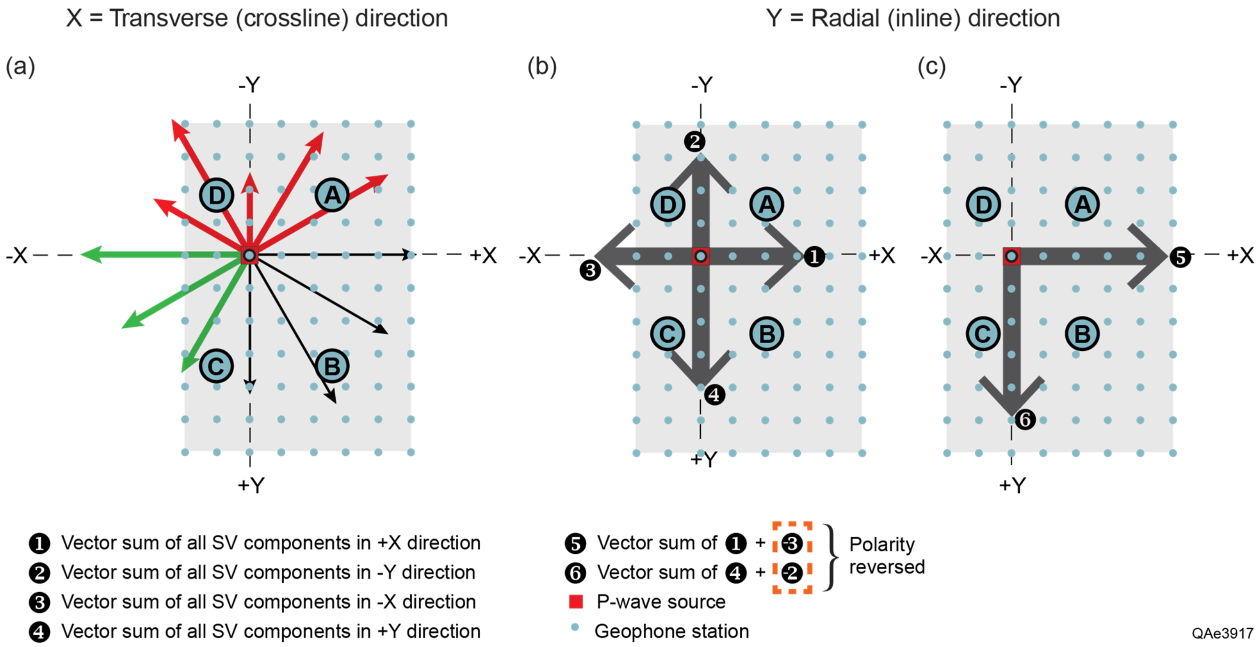

Figure 9. Converting direct-SV modes generated by a vertical-displacement source to the same polarity as S-S data created by two orthogonal horizontal-displacement sources. (a) Direct-SV rediation by a P-wave source. (b) Simplified version of P-source direct-SV radiation pattern. (c) Conversion of radiation pattern (b) to radiation pattern produced by two orthogonal horizontal vibrators.

It is essential to emphasize that the procedure described here applies only to 3D data acquisition. The extension of S-S data polarity concepts to 2D data acquisition and to vertical seismic profiling will follow in later sections. The 3C receiver stations deployed around each source station are indicated by the grid of small dots labeled in Figure 9. It will be assumed that a talented seismic field crew deployed 3C geophones so that consistent horizontal-geophone orientations exist in the inline (**Y**) direction and in the crossline (**X**) direction at each receiver station.

The multi-azimuth direct-SV radiation in Figure 9a can be viewed as a family of vectors in which each vector has a component that projects onto the crossline data-space axis (**X**) and a component that projects onto the inline data-space axis (**Y**). The sum of all of these projected vector components is represented by vectors **1, 2, 3, 4** in Figure 9b. This simpler description of direct-SV radiation from a vertical-displacement source station maintains the opposite-offset polarity and azimuth-dependent physics of the direct-SV radiation produced by a P-wave source, and allows S-S data polarity produced by vertical-displacement sources to be described in terms of data recorded by inline and crossline horizontal geophones.

The objective is to adjust the polarity of S-S data across the full 3D receiver spread so that the direct-SV radiation from a P-wave source station looks like it was created by two orthogonal horizontal vibrators. First, the algebraic sign of data recorded by the inline horizontal geophones in **-Y** space (quadrants **A** and **D**) is reversed to make the polarity of those data agree with the data polarity recorded by the inline horizontal geophones in **+Y** space (quadrants **B** and **C**). The effect of this first data-polarity adjustment is to rotate SV displacement vector **2** that points into **-Y** source (Figure 9b) space so that it is oriented in the same direction as SV vector **4** that points into **+Y** data space. The result is vector **6** in Figure 9c.

Next, the algebraic sign of data recorded by crossline horizontal geophones in **-X** space (quadrants **C** and **D**) is reversed to make the polarity of those negative-offset data agree with the data polarity of positive-offset data recorded by crossline horizontal geophones in **+X** space (quadrants **A** and **B**). This second polarity adjustment is done by rotating SV displacement vector **3** (Figure 19b) that points into **-X** source space so that it is oriented in the same direction as SV vector **1** that points into **+X** data space. The result is vector **5** in Figure 9c. These two polarity reversal actions cause the S-S data polarity across the complete 3D receiver spread to appear as if the data generated at this one source station were created by two orthogonal horizontal-displacements as shown in Figure 9c.

Thus this simple procedure of reversing the polarity of horizontal-geophone data in negative-offset-inline and negative-offset-crossline directions away from a P-wave source station causes the direct-S radiation from that P-wave source to appear on a 3D spread of receivers as if the data were generated by two orthogonal horizontal vibrators, which is the common source deployment that is used to generate S-S data. To construct 3D S-S images, this data-polarity adjustment must be done at every P-source station across a 3D survey area. Consistent definitions of *inline*, *crossline*, *negative-offset*, *and positive-offset directions* must be maintained when implementing this polarity adjustment procedure.

Data processors have great flexibility in selecting the azimuths of inline and crossline directions when they create S-S images with P-source data. For example, the inline/crossline directions used in Figure 9a are repeated in Figure 10a to illustrate how that arbitrary choice for inline and crossline directions can be easily altered to new inline/crossline azimuths incremented by angle $\boldsymbol{\Theta_1}$ (Figure 10b) or by angle $\boldsymbol{\Theta_2}$ (Figure 10c). When the polarities of data recorded by negative-offset inline and crossline horizontal geophones, as defined by these three choices of radial and transverse directions, are reversed as illustrated in Figure 9, the resulting S-S data polarities are equivalent to data polarities that would be generated by two orthogonal horizontal vibrators oriented as shown, respectively, in Figures 10d, 10e, and 10f.

If data processor #1 wants inline/crossline (i.e., radial/transverse) directions to be those shown in Figure 10b, then those choices of inline and crossline azimuths must be utilized at every P-source station across the 3D seismic grid to create S-S data polarity across the 3D data space that is consistent with that which would be created by the two orthogonal horizontal-displacement sources shown in Figure 10e. The horizontal geophones at each receiver station must also be mathematically rotated to new coordinate axes that cause a consistent horizontal geophone to be oriented in the preferred inline azimuth, and its companion horizontal geophone to be oriented in the preferred crossline direction. If data processor #2 chooses to have inline and crossline directions be those in Figure 10c, then again those definitions of inline and crossline azimuths must be enforced for all source stations and all receiver stations across the complete seismic survey area.

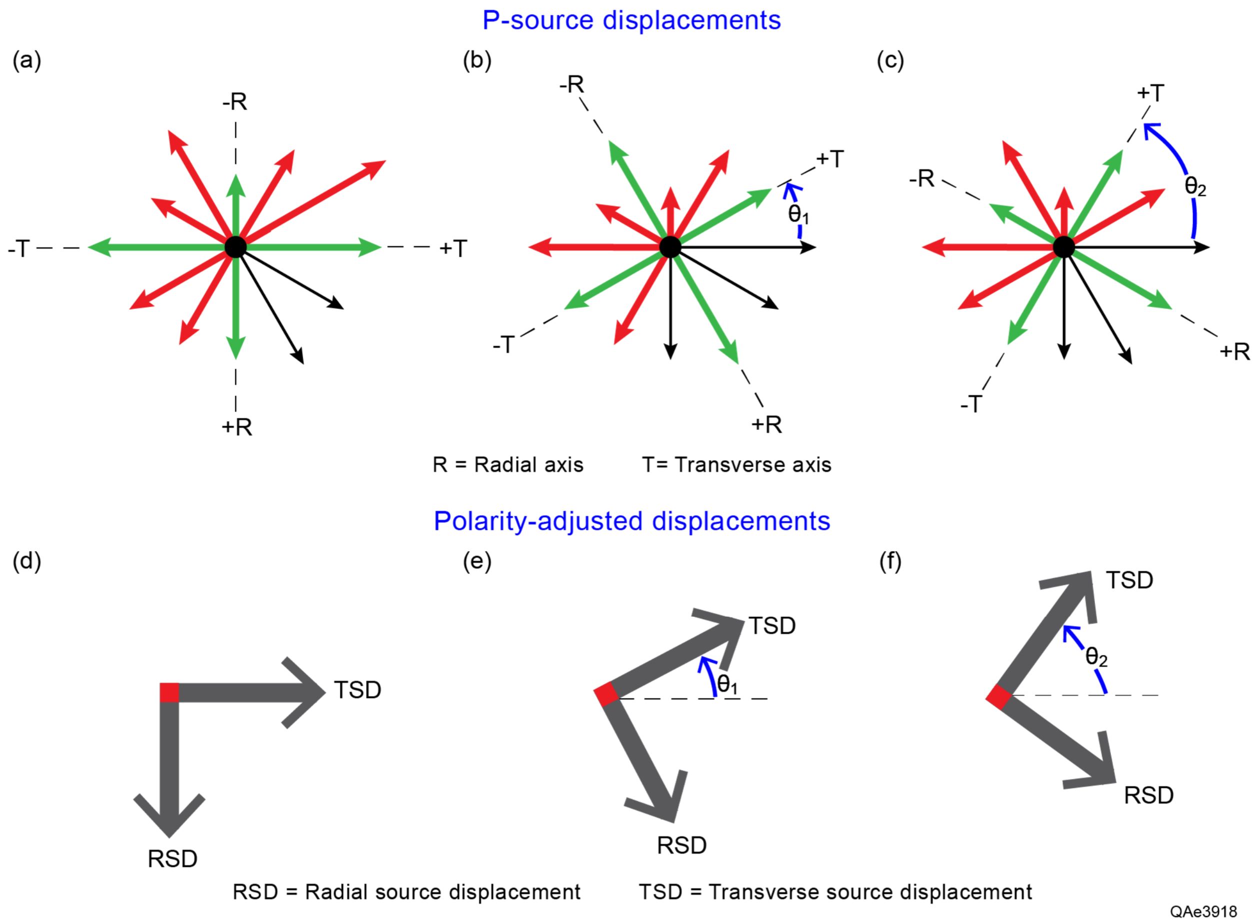

Figure 10. Direct-SV modes created by a P source allow great flexibility in selecting inline and crossline directions across seismic image space. For example three arbitrary choices for inline/crossline azimuths are shown in these panels. Once a choice of inline and crossline directions is made, then horizontal geophones at all receiver stations across a 3D survey must be mathematically rotated to those azimuths in order to perform the polarity adjustments described in Figure 9.

Extension to 2D and VSP S-S Data Processing

2D S-S Profiles

The procedure illustrated in Figure 9 applies only to 3D data generated by a P-wave source and recorded by 3C geophones. When P-source data are recorded by a 2D line of 3C geophones or by a VSP array of 3C geophones, the full benefit of adjusting the polarity of the direct-SV modes produced by a P-wave source cannot be realized as has been illustrated. For a 2D profile of surface-based 3C geophones and P-wave sources, the inline (**+Y, -Y**) data polarity adjustment illustrated in Figures 9 can be (and must be) done at every source station. For each source station, when the polarity of negative-offset data recorded by inline horizontal geo-phones (**-Y**) along a 2D profile is reversed to agree with the polarity of positive-offset inline (**+Y**) horizontal geophones, the inline S-S data are equivalent to data generated by an inline horizontal vibrator (rector 6 of Figure 9c). This polarity adjustment of inline horizontal-geophone data must be performed at every P-wave source station along a 2D profile.

However, the data-polarity adjustment of the crossline (**X** axis) horizontal geophones illustrated in Figure 9 cannot be done because no receivers are distributed orthogonal (crossline) to a 2D profile. Thus a consistent S-S crossline data polarity cannot be established along a 2D profile. At one P-source station, the vector sum of crossline SV displacements **1** and **3** drawn in Figure 9b (which is vector **5** in Figure 9c) may point in the positive-offset **+X** direction. At the next P-source station vector **5** may point in the negative-offset **-X** direction, and at the next P-source station vectors **1** and **3** may be equal amplitude and cancel each other. The result is the same as if the driver of the horizontal vibrator that was to create a crossline displacement at each source station was intoxicated and could not decide which way to orient the vibrator at each source station nor which source stations had, or had not, been visited. Thus S-S imaging along a 2D profile with P-source direct-SV modes may have to be limited to the same imaging that would be done if only an inline radial-horizontal vibrator was used to generate the data. Certainly attempts should be made to process 2D S-S data recorded by transverse-horizontal geophones. However, if questionable results are observed, this intoxicated vibrator driver analogy may in fact describe the data condition along that 2D profile, and attempts to process transverse-horizontal-geophone data may have to be abandoned.

Because azimuthal anisotropy exists to some degree across all prospect areas, this constraint that S-S data produced by a vertical vibrator along a 2D profile are equivalent to S-S data generated by only a radial-horizontal (inline) vibrator is not as restrictive as one may assume. When azimuthal anisotropy is present, a radial SV displacement will segregate into orthogonal fast-S and slow-S displacements, and these fast/slow modes will be recorded by both inline and crossline horizontal geophones along a 2D profile. Thus data recorded by both radial-horizontal and transverse-horizontal geophones will have to be processed unless the rare condition exists that the 2D profile is exactly aligned with either the fast-S or slow-S azimuth. When the azimuth of a 2D profiles does not align with fast or slow azimuths, then it should be possible to make fast and slow S-S images just as when processing radial-horizontal and transverse-horizontal data generated with two orthogonal horizontal vibrators along a 2D profile.

VSP S-S Imaging

Walkaway VSP Profiing

The comments in this section assume VSP receivers are deployed in a vertical well. Thus in map view, all 3C receivers are located at the same X,Y coordinates. There are no receivers deployed in either inline or crossline directions as in 3D imaging, or in only an inline profile as in 2D imaging. Thus S-S imaging of VSP data generated by a P-wave source is subjected to more constraints than is any other S-S imaging geometry. When S-S imaging involves a walkaway profile of P-wave source stations, none of the polarity adjustments illustrated in Figure 9 can be done because all receivers are at a single X-Y coordinate and there are no other receivers at any other crossline or inline coordinates that can contribute to controlling S-S data polarity and constructing S-S images. Only the radial SV displacements that are oriented toward the VSP well will travel to the VSP receivers. For example in Figure 9b, if a vertical VSP well is positioned in the radial positive-offset direction (**+Y**) from a P-wave source station, then the VSP receivers “see” only inline direct-SV displacement **4** (Figure 9b) because SV displacement **2** is associated with direct-SV modes that propagate away from the well. Thus, the radial (inline) sum of the positive-offset SV displacements at each walkaway P-source station will be oriented toward the VSP well as shown by vector **6** in Figure 9c, which will result in a consistent radial-S polarity along the complete VSP walkaway profile.

In contrast, the transverse (crossline) SV polarity at each walkaway P-source station is defined by the direction in which the sum of opposite-direction crossline SV displacements **1** and **3** in Figure 9b (which is vector **6** in Figure 9c) is oriented at each source station. The direction of vector **6** may be in the +**X** direction at one source station, then in direction **-X** at the next source station, and be zero at the next source station Thus there is no guarantee that there will be a consistent transverse (crossline) SV polarity along a VSP walkaway profile of P-wave sources.

<u>Single Source Far-Offset VSP</u>

The polarity situation simplifies when VSP data acquisition involves only one offset source station. When there is only one source station, the vector sum of the radial SV components that point at the VSP receiver array defines the radial-S polarity (displacement **4** in Figure 9b). The SV displacements that point away from the VSP well (vector **2**) propagate away from the receiver well and do not affect VSP radial-S polarity. The vector sum of crossline SV displacements **1** and **3** in Figure 9b defines the crossline SV polarity. In most VSP applications, it is not important what the radial-S and transverse-S polarities are because S-S data polarity can be adjusted to agree with whatever calibration data are available at a VSP well. In most instances, full S-S imaging can be done with single-source, far-offset VSP data. The exceptions will be those rare cases where transverse SV displacements **1** and **3** cancel and there is no, or only weak, transverse-S displacement created at the P-source station.

<u>Zero-Offset VSP</u>

A puzzling aspect of direct-S data observed in zero-offset VSP data generated by P-wave sources is that sometimes the downgoing direct-S first arrival is robust on both radial and horizontal geophones, sometimes it is robust on one of the rotated horizontal geophones but not on the companion horizontal geophone, and sometimes the S energy is too weak to be used for imaging purposes. This inconsistent direct-S illumination behavior for zero-offset VSP data can be explained by the direct-SV patterns illustrated in Figure 9.

In a zero-offset VSP geometry, 3C geophones will be directly below the source station (assuming a vertical receiver well). The direct-S radiation that propagates straight downward is described by the collection of SV source displacements sketched in Figures 9a and 9b. At some well locations vectors **1, 2, 3, 4** in Figure 9b sum to create robust versions of the two orthogonal displacement vectors **5** and **6** in Figure 9c. In this case, strong S-wave first arrivals are observed on both horizontal geophones in zero-offset VSP data. In some instances SV displacement vectors **1, 2, 3, 4** (Figure 9b) may sum so that either SV vector **5** or vector **6** (Figure 9c) is almost zero. In such a case, one downhole, zero-offset, horizontal geophone may record a respectable response, but the companion horizontal geophone may record no response. If SV displacements **1, 2, 3, 4** sum so that trivial-amplitude versions of displacements **5** and **6** are created, then no downgoing direct-S will be observed in zero-offset VSP data.

Thus the quality of direct-S data that a P-wave source creates in zero-offset VSP data is not predictable. The downgoing direct-S wavefield may be robust, weak, or non-existent depending on the nature of the azimuthal irregularity in the direct-SV radiation pattern shown in Figure 9a. To ensure that a robust direct-S wavefield is generated, it is essential that the radiation pattern in Figure 9a have large azimuth variations in amplitude. This irregular azimuth behavior requires that there be azimuth variations in the stiffness coefficients local to the P-wave source station. Physical features near a zero-offset source station that create variations in stiffness coefficients include: abrupt changes in surface topography, tree roots, boundaries between a soft surface and a hard surface, mud pits, farm ponds, gullies, small streams, man-made ditches, etc. VSP engineers should utilize the physical presence of such features to ensure that there will be an azimuth-dependent variation in the direct-SV displacements produced by a vertical-displacement source at a near-offset position.

SV-P Imaging

SV-P Data Polarity

The opposite-polarity behavior of P-source S-S data recorded by negative-offset and positive-offset horizontal geophones is caused by the opposing orientations of the horizontal components of SV displacement vectors **C** and **D** shown in Figure 1c. The offset-direction polarity behavior of SV-P data differs from that of S-S data because the polarities of upgoing converted-P reflections are established by the vertical components of SV displacements **C** and **D** (Figure 1c), not by the horizontal components of these vectors. The vertical components of **C** and **D** point in the same direction (upward) so opposite-azimuth SV-P reflections have identical polarities (Figure 2b). Thus no polarity corrections of negative-offset data are required for SV-P imaging with vertical-displacement sources like has to be done for S-S data generated by these same sources (Figure 2c).

Topic 2: SV-P Velocity Analysis

The material in this section is not intended to be a thorough treatise on direct-S velocity analysis. The single objective is to describe a procedure that aids in recognizing SV-P reflections in common-midpoint (CMP) constant-velocity stacks used to determine P-P stacking velocities. When these SV-P reflections are identified in velocity analyses that are intended to define P-P imaging velocities, two vital pieces of information become available:

1. There is assurance that SV-P reflections exist in the vertical-geophone data, and preliminary conclusions can be made about the signal-to-noise quality of those reflections.

2. When several SV-P reflections can be identified across a panel of P-P CMP-based constant-velocity stacks a tentative SV-P stacking velocity is defined for the XY image coordinates where the P-P CMP velocity panel was constructed.

The knowledge provided by these insights is invaluable. Specifically, a data processor can now decide if there is justification for SV-P velocity analysis to be expanded out of CMP image space into asymptotic-conversion-point (ACP) image space where SV-P stacking velocities can be determined with more precision. The important point is that even though SV-P data should be analyzed by applying ACP binning procedures to vertical-geophone data, vital SV-P stacking velocity information can still be determined from CMP constant-velocity stacks of those same vertical-geophone data. A key requirement is that these CMP constant-velocity stacks must extend to slower P-wave velocities than what some data processors consider when estimating P-P imaging velocities. Thus velocity panels used to construct some legacy P-P data volumes may have to be redone to ensure that a range of slow stacking velocities is available that is adequate to reveal SV-P reflection events.

A V_P/V_S velocity ratio that is appropriate for the imaging area that is being considered is needed in this application. This ratio may be determined from dipole sonic logs, VSP data, velocity measurements on core samples, or published velocity data for similar rocks. In some cases, a data processor may have to simply assume a value for the V_P/V_S ratio at a particular prospect area if no information about S-wave velocity is available. The V_P/V_S value that is used should represent the velocity ratio for the deeper rocks that will be imaged because the ratio value will be used to determine the SV-P velocity associated with ACP binning. By definition, ACP binning is appropriate for stacking converted-mode data only in the lower half (or two-thirds) of SV-P imaging space. Thus assuming a V_P/V_S ratio is not as challenging or as risky as might be thought. A ratio value of 2 will be approximately correct in many instances. The illustration in Figure 11 summarizes how a SV-P velocity analysis can be done with CMP constant-velocity stacks when a V_P/V_S velocity ratio is established by any of these options.

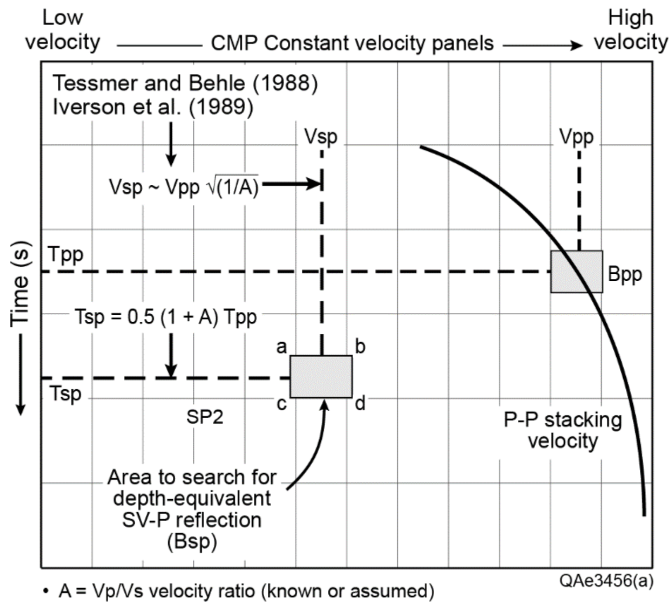

- A = Vp/Vs velocity ratio (known or assumed)
- Bpp = Good-quality P-P reflection
- Bsp = SV-P reflection depth equivalent to Bpp
- abcd = Area to search for Bsp
- (Tpp, Vpp) = P-P image time and stacking velocity for Bpp
- (Tsp, Vsp) = Estimated SV-P image time and stacking velocity for Bsp

Figure 11. A simple procedure for determining reasonably accurate SV-P stacking velocities from P-P stacking velocities. The hypothetical constant-velocity stack panel shown here are CMP gathers constructed from vertical-geophone data at a specific CDP coordinate in P-P image space. A specific P-P reflection $\mathbf{B_{PP}}$ at P-P image time $\mathbf{T_{PP}}$ is indicated on the P-P stacking velocity curve at velocity panel $\mathbf{V_{PP}}$. The depth-equivalent SV-P reflection $\mathbf{B_{SP}}$ occurs on velocity panel $\mathbf{V_{SP}}$ at time coordinate $\mathbf{T_{SP}}$. The two equations written on the velocity panel define a region **abcd** where reflection $\mathbf{B_{SP}}$ should be positioned (if that reflection exists).

The approach to SV-P velocity analysis described here does not seem to be widely used, probably because of the reluctance to think that ACP-based reflection events (SV-P reflections) will appear in a data product created for the purpose of recognizing CMP-based reflections (P-P reflections). Two simple equations are utilized to recognize the presence of SV-P primary reflections in P-P constant-velocity stacks. The first equation was proposed by Tessmer and Behle (1988) and by Iverson, et al. (1989) and is stated as Equation 1:

(1) $V_{SP} = V_{PP}\,(1/A)^{1/2}$.

In this equation $\mathbf{V_{SP}}$ is the SV-P stacking velocity for a SV-P reflection from a particular interface, $\mathbf{V_{PP}}$ is the P-P stacking velocity for a P-P reflection from that same interface, and **A** is the average or RMS V_P/V_S velocity ratio extending to the target interval. There is rarely a significant difference in average and RMS velocity ratios. This equation was developed for the converted-SV mode (P-SV). However, the equation can also be used for the converted-P mode (SV-P) because $\mathbf{V_{SP}}$ and $\mathbf{V_{PS}}$ velocities are equivalent in propagation media that do not have extreme lateral variations in layer velocities. The second equation that is needed is:

(2) $T_{SP} = (0.5)\ T_{PP}\ (1 + A)$.

This equation expresses the relationship between a P-P reflection that occurs at P-P image time $\mathbf{T_{PP}}$ and the depth-equivalent SV-P reflection that occurs at SV-P image time $\mathbf{T_{SP}}$. Again **A** is the average or RMS V_P/V_S velocity ratio.

A broad suite of hypothetical CMP constant-velocity stacks of vertical-geophone data is depicted in Figure 11. These velocity stacks are calculated at one common-depth-point (CDP) in P-P image space. The P-P stacking velocity appropriate for this CDP position is shown curving across the higher velocity portion of the stack panels, and one primary P-P reflection $\mathbf{B_{PP}}$ is emphasized on velocity panel $\mathbf{V_{PP}}$. The challenge is to determine if a SV-P reflection $\mathbf{B_{SP}}$ that is depth-equivalent to $\mathbf{B_{PP}}$ also exists in the stack panels. Equation 1 defines the approximate velocity panel $\mathbf{V_{SP}}$ where reflection $\mathbf{B_{SP}}$ should be, and Equation 2 defines the approximate time coordinate where reflection $\mathbf{B_{SP}}$ should be positioned on that velocity panel. The result is that a general search window **abcd** is created which can then be inspected to determine if a flat reflection is present. If such a flat reflection is found, *it should be assumed to be a SV-P primary reflection*. Traditional data-processing philosophy has been to assume that any flat reflections found within area **abcd** is a P-P multiple. Such a reflection may indeed be a P-P multiple. However, the assumption that the event is a P-wave multiple rather than a SV-P primary reflection should be made ***only*** if evidence is provided to support that assumption. An argument for a P-P multiple must be based on evidence that is equal to, or superior to, the evidence provided by Equations 1 and 2 that the event is a SV-P primary reflection.

How large should the search area **abcd** in Figure 11 be? There is no set answer for this question. Each data processor will have a different opinion about the size of the search area. Each data processor will also become comfortable about the lateral and vertical search dimensions used for coordinates $\mathbf{V_{SP}}$ and $\mathbf{T_{SP}}$ that they will allow for different propagation media as they gain more experience in processing SV-P data.

If this analysis procedure causes three or more P-P primary reflections along the indicated P-P stacking-velocity curve to be associated with flat events on slower-velocity panels, then a tentative SV-P stacking velocity for the CDP coordinate can be created. Real data examples of using this procedure to establish relationships between P-P and SV-P stacking velocity curves are presented as Figures 12 and 13. The constant-velocity stacks of vertical-geophone data in Figure 12 are CMP-based because the purpose was to determine P-P stacking velocity. The SV-P stacking velocity curve defined by calculating $\mathbf{V_{SP}}$ and $\mathbf{T_{SP}}$ coordinates from $\mathbf{V_{PP}}$ and $\mathbf{T_{PP}}$ coordinates with Equations 1 and 2 is positioned across the constant-velocity stacks, and depth-equivalent P-P and SV-P reflections are emphasized. This is a real-data example of estimating an SV-P stacking function from P-P stacking velocities determined by CMP procedures applied to vertical-geophone data. The calculated positions of two S-S reflections that are depth-equivalent to selected P-P and P-SV reflections are labeled on curve SV-SV.

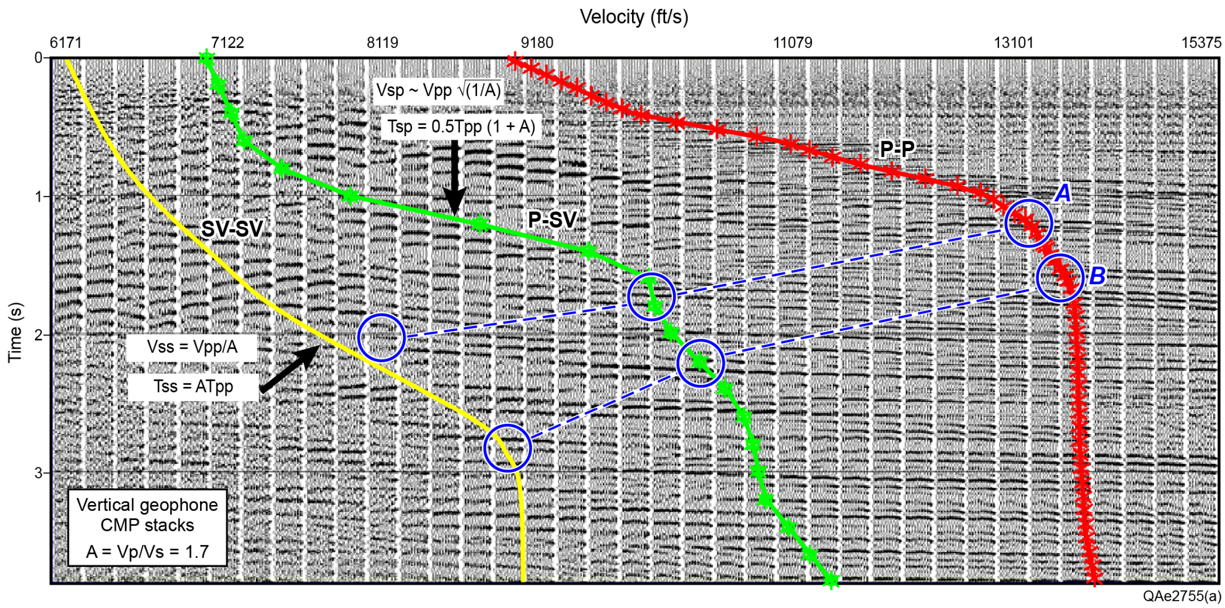

Figure 12. CMP constant-velocity stacks of vertical-geophone data. These data panels were created for constructing P-P stacking velocities. The relationships defined by Equations 1 and 2 are used to define where SV-P primary reflections should be located that are depth-equivalent to the selected P-P primary reflections. Curve SV-SV is the calculated position of depth-equivalent S-S reflections.

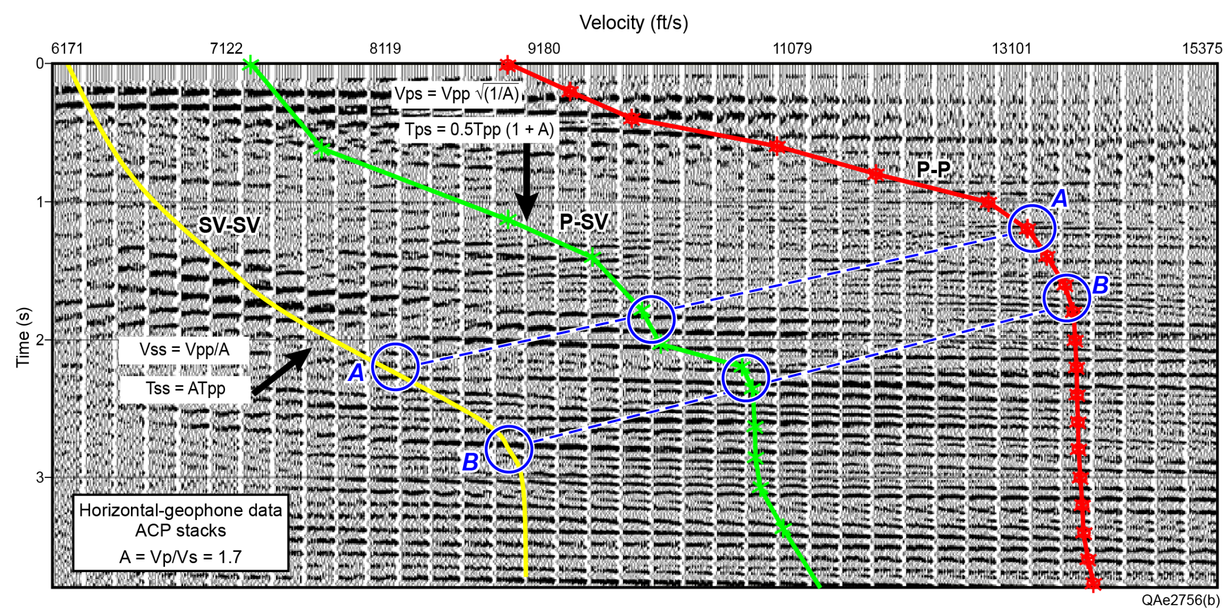

Figure 13. ACP constant-velocity stacks of horizontal-geophone data. These data panels were created for determining SV-P stacking velocities. The relationships defined by Equations 1 and 2 are used to define where P-P primary reflections should be located that are depth-equivalent to the selected SV-P primary reflections. Curve SV-SV is the calculated position of depth-equivalent S-S reflections.

In contrast, the constant-velocity stacks of horizontal-geophone data in Figure 13 are ACP-based because the purpose was to determine P-SV stacking velocities. For the geology where these data were acquired, SV-P velocities should be approximately the same as P-SV velocities. The P-P stacking velocity curve defined by calculating $\mathbf{V_{PP}}$ and $\mathbf{T_{PP}}$ coordinates from $\mathbf{V_{SP}}$ and $\mathbf{T_{SP}}$ coordinates with Equations 1 and 2 is identified, and depth-equivalent P-P and SV-P reflections are emphasized. This is an example of estimating CMP-based P-P stacking velocities from ACP-based SV-P stacking velocities. The calculated locations where two S-S reflections would be that are depth-equivalent to their companion P-SV reflections are labeled on curve SV-SV.

Conclusions

Creating S-S images from direct-SV data generated by vertical-displacement sources requires that data-processing procedures be done that are not necessary when creating S-S images from horizontal vibrator data. The principal difference in direct-S modes produced by horizontal-displacement and vertical-displacement sources is the contrast in the azimuth behavior of direct-S data polarity produced by these two classes of seismic sources. Direct-SV modes propagating in opposite-azimuth directions from a vertical-displacement source station have opposite polarities on horizontal geophones. In contrast, direct-S modes propagating in opposite-azimuth directions from a horizontal vibrator have identical polarities on the same horizontal geophones. When the data-processing objective is to create S-S images, this wave physics requires that the algebraic sign of vertical-displacement-source data that are recorded by negative-offset horizontal geophones be reversed. This simple data-processing step causes negative-offset and positive-offset S-S data around a vertical-displacement source station to have the same polarities that a horizontal-vibrator source would create. S-S data processing can then proceed just as it does for horizontal-vibrator data.

In contrast to S-S imaging with P-wave sources and horizontal geophones, no data polarity adjustments are required when performing SV-P imaging with P-wave sources and vertical geophones. Because SV-P data are recorded by vertical geophones, the data propagating away from each source station have the same polarity at receiver stations positioned in all negative-offset and positive-offset azimuth directions away from a P-wave source station.

Two simple equations that relate the NMO velocities and zero-offset arrival times of depth-equivalent P-P and SV-P reflections allow CMP-based P-P constant-velocity stacks of vertical-geophone data to provide two important pieces of information needed for ACP-based SV-P imaging. First, SV-P reflections, which should be created with ACP binning procedures, can be identified in a P-P constant-velocity panel constructed from vertical-geophone data even though the P-P velocity panels are constructed with CMP binning procedures. By recognizing these SV-P reflections, information is provided that justifies efforts to proceed with SV-P data processing. Second, tentative SV-P stacking velocity curves can be constructed if sequences of SV-P reflections are discovered in P-P velocity analyses at several CDP locations. By such examinations of CMP-based P-P velocity analysis panels, data processors are far ahead in knowledge when they initiate serious ACP-based velocity analysis to construct SV-P stacking velocities.

References

Guy, E.D., 2004, Evaluation of near-surface converted-mode seismic reflection imaging potential: Electronic Journal of Geotechnical Engineering, v. 9, p. 1-35.

Hardage, B.A., and D. Wagner, 2014a, 2-D modeling of direct-S and direct-P wavefields – part 1 – modeling principles and examples: EGL Sponsor Report, Members Area of EGL Web site.

Hardage, B.A., and D. Wagner, 2014b, 2-D modeling of direct-S and direct-P wavefields – part2 – P and S radiation patterns: EGL Sponsor Report, Members Area of EGL Web site.

Iverson, W.P., B.A. Fahmy, and S.B. Smithson, 1989, V_PV_S from mode converted P-SV reflections: Geophysics, v. 54, p. 843-852.

Miller, G., and Pursey, H., 1954, The field and radiation impedance of mechanical vibrators on the free surface of a semi-infinite isotropic solid: Proceedings of the Royal Society of London, Series A, v. 223, no. 1155, p. 521-541.

Tessmer, G., and A. Behle, 1988, Common reflection point data-stacking technique for converted waves: Geophys. Prosp., v. 36. P. 671-688.

White, J.E., 1983, Underground sound – applications of seismic waves: Elsevier Science Publishers.